GRC: Coastal Ocean Modeling 2011

Observations of submesoscale eddies using high-frequency radar-derived kinematic and dynamic quantities

Sung Yong Kim

Marine Physical Laboratory, Scripps Institution of Oceanography, La Jolla, CA 92093-0213 USA, syongkim@mpl.ucsd.edu

Abstract

The spatio-temporal variability of submesoscale eddies off southern San Diego is investigated with two-year observations of subinertial surface currents [$O(1)$ m depth] derived from shore-based high-frequency radars (HFRs). The kinematic and dynamic quantities – velocity potential, stream function, divergence, vorticity, and deformation rates – are directly estimated from radial velocity maps using optimal interpolation. For eddy detection, the winding-angle approach based on flow geometry is applied to the calculated stream function. A cluster of nearly-enclosed streamlines with persistent vorticity in time is identified as an eddy. About 700 eddies were detected for each rotation (clockwise and counter-clockwise). The two rotations show similar statistics with diameters in the range of 5 – 25 km and Rossby number of 0.2 – 2. They persist for 1 – 7 days with weak seasonality and migrate with a translation speed of 4 – 15 $\mathrm{cm\,s^{-1}}$ advected by background currents. The horizontal structure of eddies exhibits nearly symmetric tangential velocity with a maximum at the defined radius of the eddy, non-zero radial velocity due to background flows, and Gaussian vorticity with the highest value at the center. In contrast divergence has no consistent spatial shape. Two episodic events are presented with other in-situ data (subsurface current and temperature profiles, and local winds) as an example of frontal-scale secondary circulation associated with drifting submesoscale eddies.

Observations

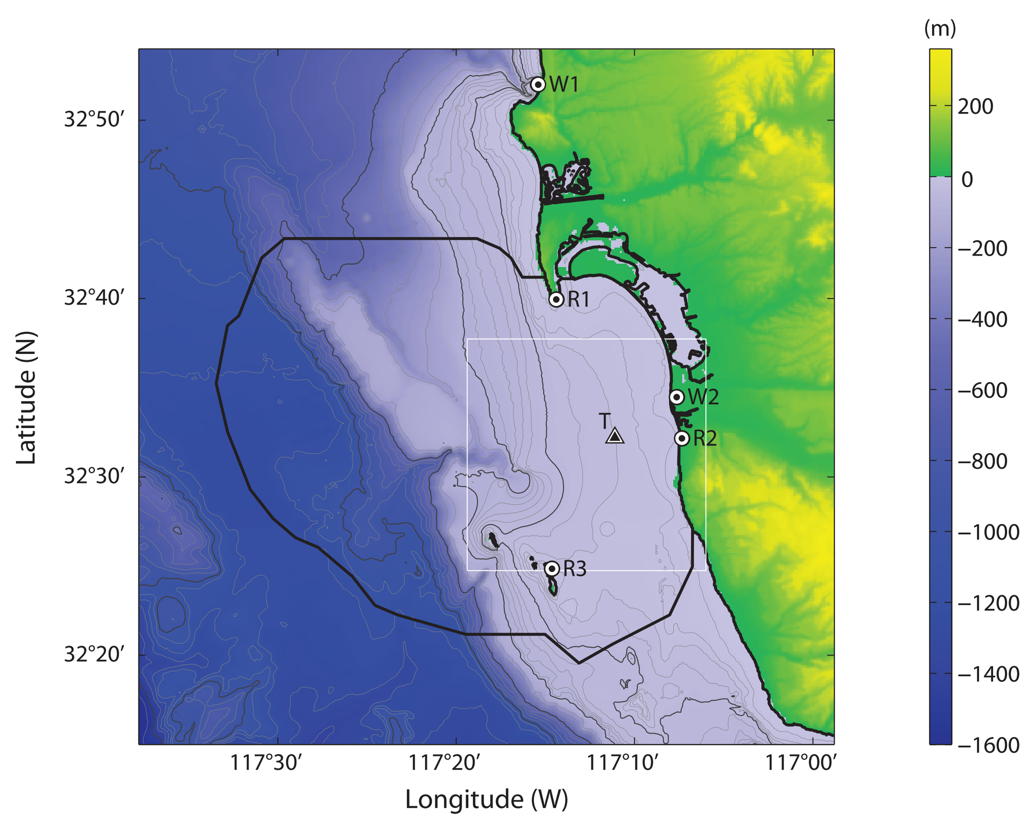

Figure 1: An observation domain of submesoscale eddies using in-situ observations: Three high-frequency radars (HFRs) [R1 (Point Loma), R2 (Imperial Beach), and R3 (Coronado Islands)] for surface currents, two stations at the Scripps Pier (W1, SIO) and Tijuana River Valley (W2, TJR) for wind, and one mooring (T) for both subsurface currents (ADCP) and temperature profile. A black outline denotes the effective coverage area of HFRs (at least 70% data availability for two years). A white square box is the area for closed-up view in Figures 3a and 3b. The bottom bathymetry contours are indicated by thin curves with 10 m ($0 < z < 100$ m) and 50 m ($100 < z < 1000$ m) contour intervals and thick curves at the 50, 100, 500, and 1000 m depths.

Eddy detection

The WA method [1] finds nearly-closed streamlines with a single rotation (clockwise or counter-clockwise). Each streamline is a set of N line segments, i.e. a polygon, and the sum (Θ) of their exterior angles (θ_k) should be $\pm 2\pi$:

$$\Theta = \sum_{k=0}^{N-1} \theta_k = \sum_{k=0}^{N-1} \angle P_{k-1} P_k P_{k+1}, \tag{1}$$

where $P_{-1} = P_N$ for a closed polygon and P_k denotes a discrete point of the polygon ($k = 0, 1, \cdots, N$).

Horizontal divergence (δ), vorticity (ζ), shearing deformation rate (ϱ), stretching deformation rate (ς), and strain rate (κ) of surface currents are

$$\delta = \nabla_H \cdot \mathbf{u} = \frac{\partial u}{\partial x} + \frac{\partial v}{\partial y}, \tag{2}$$

$$\zeta = \nabla_H \times \mathbf{u} = \frac{\partial v}{\partial x} - \frac{\partial u}{\partial y}, \tag{3}$$

$$\varrho = \frac{\partial v}{\partial x} + \frac{\partial u}{\partial y}, \tag{4}$$

$$\varsigma = \frac{\partial u}{\partial x} - \frac{\partial v}{\partial y}, \tag{5}$$

$$\kappa = \sqrt{\varrho^2 + \varsigma^2}. \tag{6}$$

The vertical rotary coefficient (α) is defined as a function of time: [2]:

$$\alpha(t) = \frac{-\sum_{m<0} S(m,t) + \sum_{m>0} S(m,t)}{\sum_{m<0} S(m,t) + \sum_{m>0} S(m,t)}, \tag{7}$$

where $S(m,t)$ is the rotary power spectrum of vertical current profile at time t and m is the vertical wavenumber. Negative ($\alpha < 0$) and positive ($\alpha > 0$) values indicate clockwise and counter-clockwise (looking down from the top), respectively.

Vertical structure

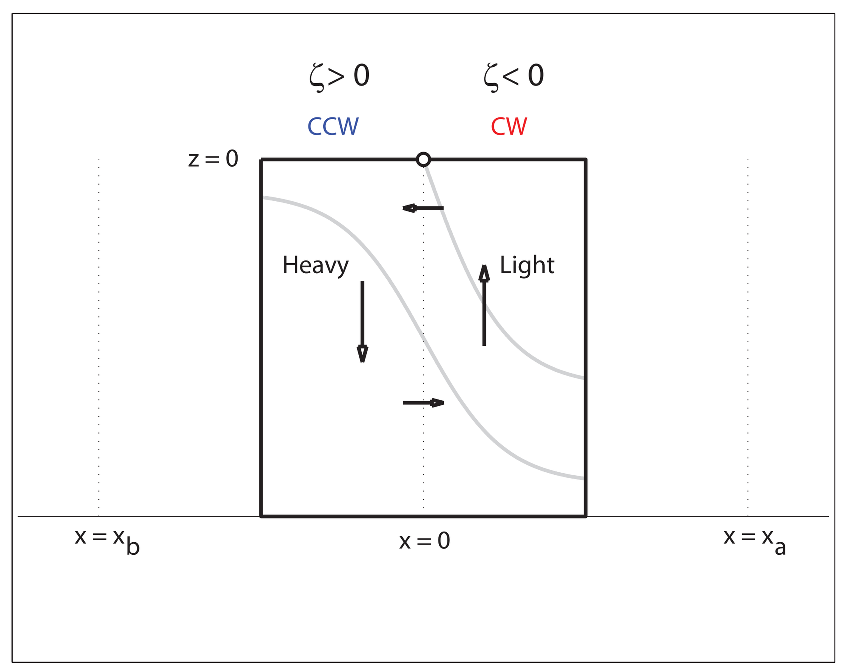

Figure 2: A schematic frontal-scale secondary circulation associated with a drifting density front (at $x = 0$ and $z = 0$) presented in the cross-front plane view [adapted from [3]]. When a jet along the density front accelerates, a secondary circulation develops in vertical as the form of upwelling on the warmer side (clockwise eddy) and downwelling on the colder side (counter-clockwise eddy) as a response to the horizontal density gradient and strain rate. The front drifts from $x = 0$ to $x = x_a$ or $x = x_b$. Gray curves are isopycnals, and the vertical coordinate (z) is positive upward.

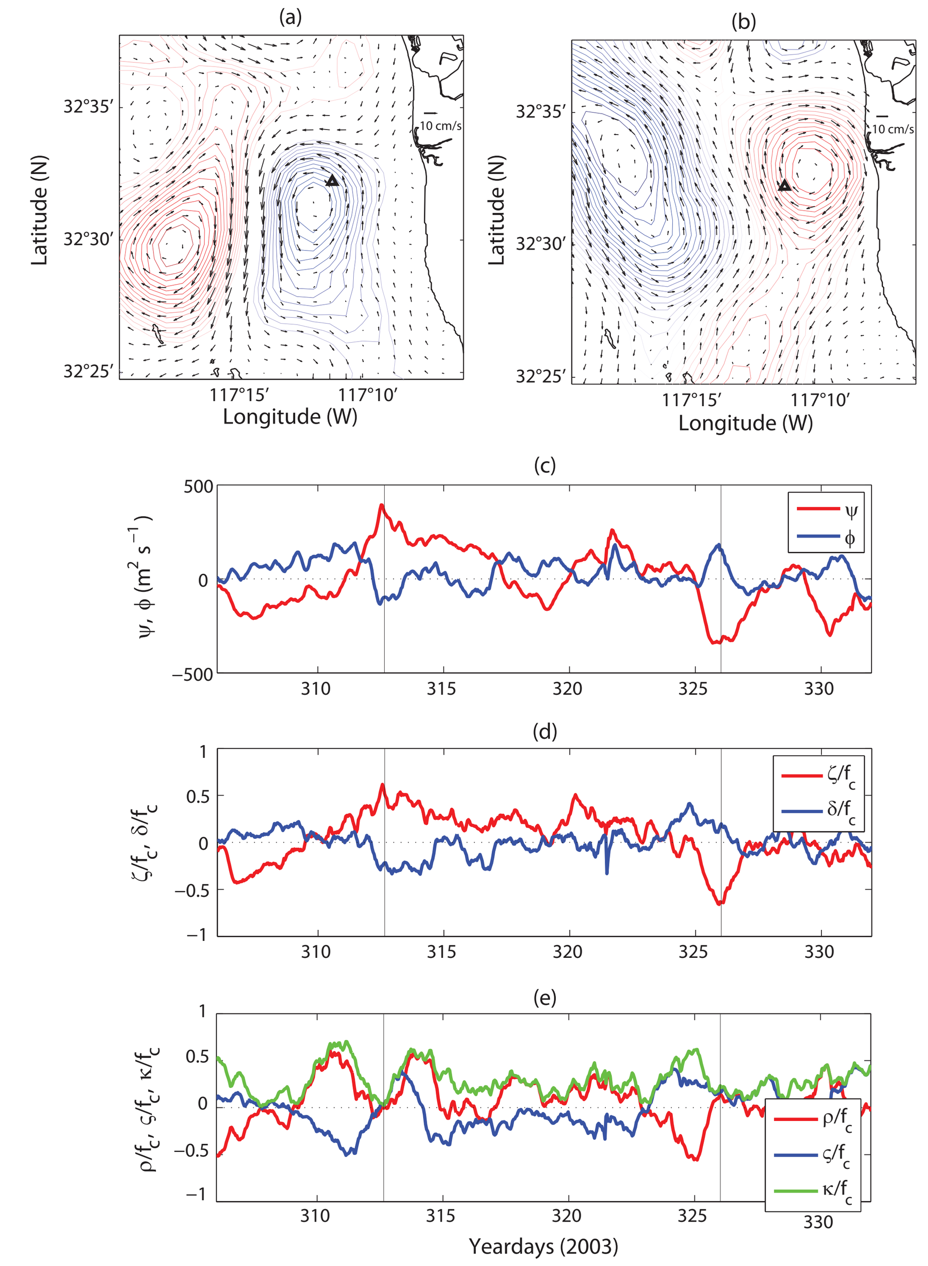

Figure 3: Vertical structure (Part I). (a) and (b): Two snapshots of stream function when counter-clockwise and clockwise eddies pass by a local mooring marked as a black triangle on 312.65 and 326.02 yeardays of 2003 (GMT), respectively, which are indicated by two vertical black lines in (c) – (d) and Figure 4. The stream function-derived surface currents ($\mathbf{u}_\psi$) are overlaid on the contours of stream function. (c) Stream function (ψ, $\mathrm{m^2\,s^{-1}}$) and velocity potential (ϕ, $\mathrm{m^2\,s^{-1}}$). (d) Normalized divergence (δ/f_c) and vorticity (ζ/f_c). (e) Normalized shearing rate (ϱ/f_c), stretching rate (ς/f_c), and strain rate (κ/f_c). (c) – (e) are values at the mooring location [a black triangle in (a) and (b)].

A clockwise eddy passes by the local mooring between 305 – 310 yeardays from northwest to southeast, followed by a counter-clockwise eddy (Figures 3c – 3e). A strong upward current raises up the thermocline (Figure 4d) when the sign of vorticity (or stream function) changes on 310 (or 311) yeardays from negative to positive (Figure 3b). At that time, the shearing rate ($\varrho > 0$) and stretching rate ($\varsigma < 0$) have their local maximum and minimum, respectively, with opposite signs (Figure 3e). As long as the local mooring is located within the core of the counter-clockwise eddy (Figures 3a and 3b), the downward currents continue ($\delta/f_c < 0$ and $\zeta/f_c > 0$). As an opposite case, a counter-clockwise eddy moves from south to northwest between 321 – 327 yeardays around the mooring (Figure 3b). The thermocline is pushed down near the time when stream function and vorticity (positive to negative) change their signs as well as velocity potential and divergence (negative to positive) do on 323.62 yeardays (Figure 4d). The local high shearing and stretching rates appear out of phase (Figure 3e). Then the thermocline moves upward, and as the influence of the clockwise eddy becomes dominant, the upwelling current slowly decelerates (Figure 4d). The maximum strain rate (κ) occurs right before high vorticity rather than at the same time (Figure 3e).

The rotary coefficient and stream function are nearly in phase except when both stream function and velocity potential have weak fluctuations (Figure 4c), which shows the rotation derived from surface currents is well aligned with vertical current rotation. These exhibit covariant subinertial currents at the surface and in the subsurface water column in a nearshore environment.

The local winds at SIO and TJR are not likely to be directly related to up/downward movements of the thermocline associated with wind-driven upwelling and downwelling (Figure 4e). The wind in this region is relatively weak (a typical wind speed is 2 – 4 $\mathrm{m\,s^{-1}}$) compared other regions on the U. S. West Coast. Therefore the integrated observations in this study are more appropriate to interpret with submesoscale process rather than classic Ekman dynamics.

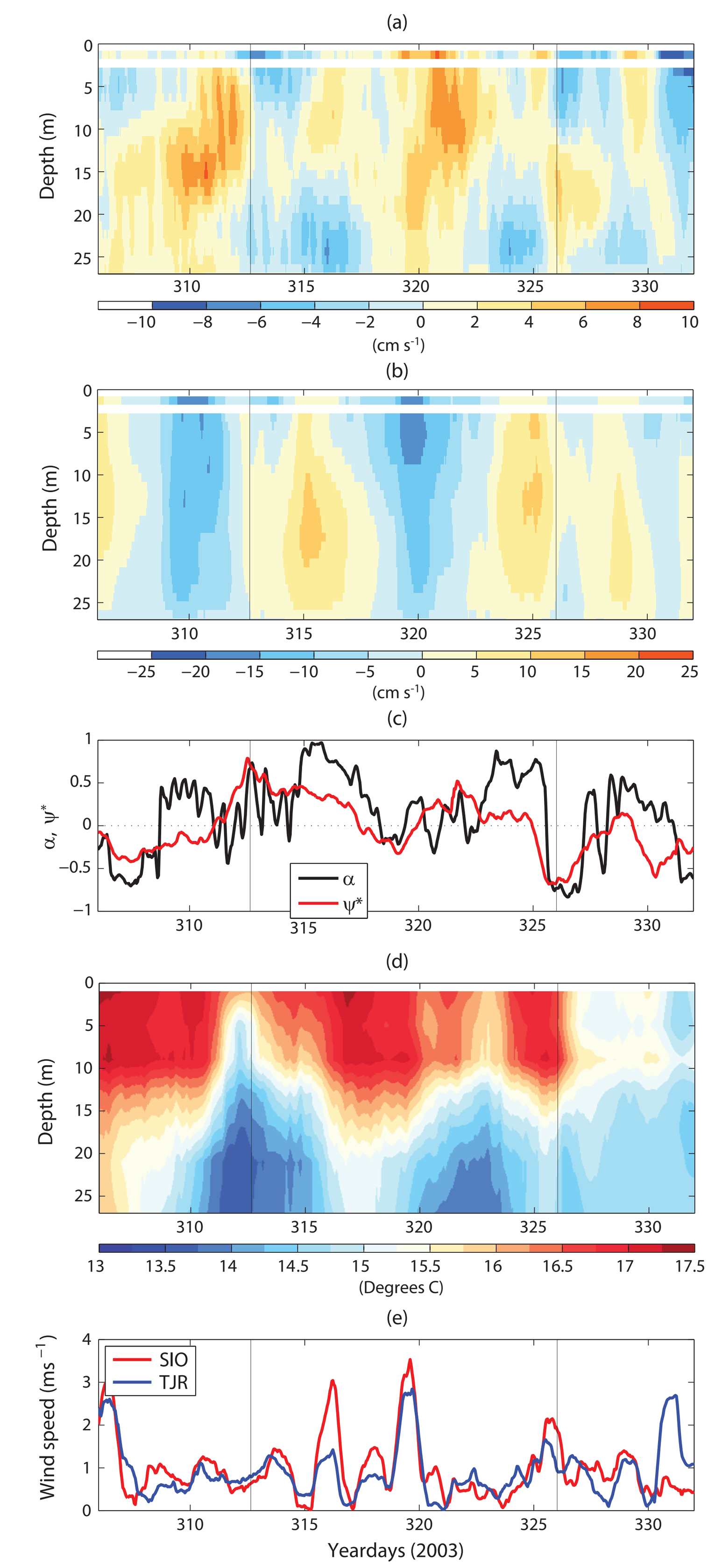

Figure 4: Vertical structure (Part II) (a) and (b): Subinertial current profile (u- and v-components). The HFR-derived surface currents are placed on the top of subsurface current profile ($\mathrm{cm\,s^{-1}}$). (c) Vertical rotary coefficient (α in equation 7) and normalized stream function ($\psi^* = \psi/\psi_0$, $\psi_0 = 500\ \mathrm{m^2\,s^{-1}}$). The negative and positive rotary coefficients denote the current profile with clockwise and counter-clockwise rotation looking down from the top. (d) Subinertial temperature profile (°C). (e) Subinertial wind speed ($\mathrm{m\,s^{-1}}$) at SIO and TJR.

Statistics of identified eddies

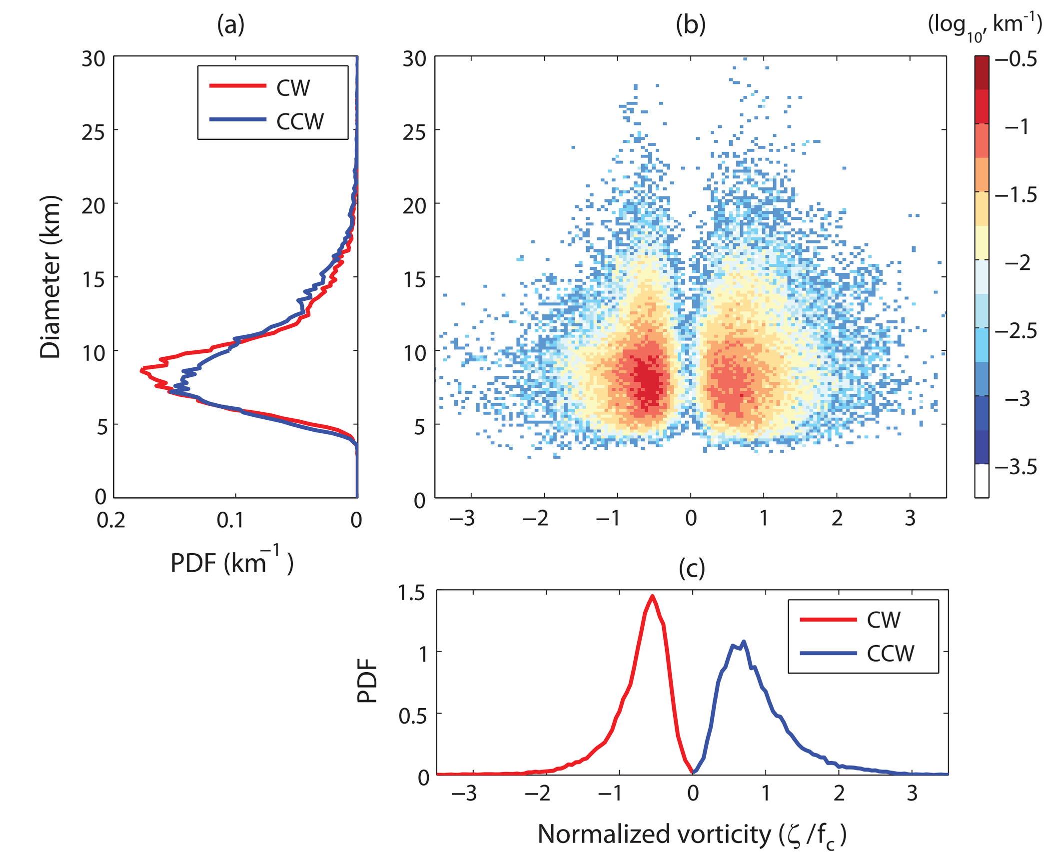

Figure 5: Probability density functions (PDFs) of (a) diameter (L) and (c) normalized vorticity (ζ/f_c) at the center of eddies. (b) Joint PDF of diameter and normalized vorticity.

Concluding remarks

Submesoscale process studies have benefited from numerical models to explain four-dimensional dynamical components in a theoretical framework. However, there are very limited in-situ observations because of the requirement for high-resolution (hourly in time and km in space) measurements of ocean surface and interior. As a part of the observational efforts, surface current measurements using high-frequency radar can provide a rich asset to substantiate the surface submesoscale process (e.g., fronts, filaments, and eddies) and to find the missing link between offshore and nearshore where satellite remote sensing observations are limited. On the top of that, the integrated observations with continuous time and broad spatial scales enable us to understand and interpret the real phenomena themselves.

Acknowledgement Author is supported by the Coastal Ocean Currents Monitoring Program (COCMP) from the State of California, the Office of Naval Research (ONR), and the British Petroleum (BP) through the BP Institute at Scripps Institution of Oceanography (SIO). Surface current data are provided from the Southern California Coastal Ocean Observing System (SCCOOS, Available online at `http://www.sccoos.org`) at SIO. Author appreciates discussion and supports from Bruce Cornuelle, Eric Terrill, Mark Otero, Lisa Hazard, Paul Reuter, Jen Bowen, and Tom Cook at SIO.

References

[1] I. A. Sadarjoen. *Extraction and Visualization of Geometries in Fluid Flow Fields.* PhD thesis, Delft University of Technology, 1999.

[2] K. D. Leaman and T. B. Sanford. Vertical energy propagation of inertial waves: A vector spectral analysis of velocity profiles. *J. Geophys. Res.*, 80(15):1975–1978, 1975.

[3] B. J. Hoskins and F. P. Bretherton. Atmospheric frontogenesis models: Mathematical formulation and solution. *J. Atmos. Sci.*, 29(1):11–37, 1972.